



Synthesization pill-like C-doped ZnO nano-photocatalyst for removing ofloxacin and methylene blue under visible light

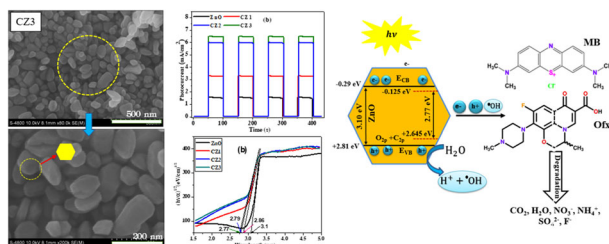
Thi Viet Ha Luu¹ · Nguyen Thi Mai Tho¹ · Tran Thi Thanh Thuy¹ · Le Nhat Thong¹ · Nguyen Trung Dung² · Phuc Huu Dang³

Received: 25 October 2023 / Accepted: 14 February 2024 / Published online: 6 March 2024
© The Author(s), under exclusive licence to Springer Science+Business Media, LLC, part of Springer Nature 2024

Abstract

Carbon-doped zinc oxides were synthesized with different concentrations corresponding to PVA/Zn²⁺ molar ratios between 5 and 15% by the hydrothermal method. The XRD and SEM results show that the obtained materials have high crystallinity and a pill-like morphology. Carbon dopant significantly decreased band gap energy ($E_{gCZ3} = 2.77$ eV), improving the optical absorption of ZnO in the visible and ultraviolet regions. Generally, the catalyst with carbon doped 1.49% (CZ3), corresponding to the molar ratio of $PVA/Zn^{2+} = 15\%$, showed the highest photocatalytic efficiency of ofloxacin (Ofx) and methylene blue (MB) and was higher than pure ZnO. This is possibly attributed to its morphology with good uniformity and porosity; the specific surface area of SCZ3 is 26 m²/g which is 1.5 times higher than ZnO. Moreover, it is also relative to the stable and highest saturation photocurrent density of CZ3, which is ~ 6.4 $\mu A \cdot cm^{-2}$, 4.15 times higher than pure ZnO. In addition, trapping experiments showed that positive holes and hydroxyl radicals were the predominant active agents. Finally, COD and TOC analysis results suggested that the photodegradation progress of MB and Ofx formed organic compounds with smaller structures and proved that over 78% of MB and 66% of Ofx were converted entirely to simple inorganic substances such as CO₂, H₂O, etc.

Graphical Abstract



Keywords C-doped ZnO · Polyvinyl alcohol · Ofloxacin · Visible light · Photocatalyst · Hydrothermal method

✉ Thi Viet Ha Luu
luuthivietha@iuh.edu.vn

✉ Phuc Huu Dang
danghuuphuc@iuh.edu.vn

¹ Faculty of Chemical Engineering, Industrial University of Ho Chi Minh City, Ho Chi Minh City 70000, Vietnam

² Department of Chemical Engineering, Le Quy Don Technical University, 236 Hoang Quoc Viet, Hanoi 100000, Vietnam

³ Faculty of Fundamental Science, Industrial University of Ho Chi Minh City, Ho Chi Minh City 70000, Vietnam

Highlights

- The pill-like nano-photocatalysts of C-doped ZnO (CZ) were prepared by the hydrothermal method with various PVA/Zn²⁺ molar ratios (5, 10, and 15%).
- The C doping significantly decreased the band gap of pure ZnO (from 3.1 to 2.77 eV).
- Enhancing the photoinduced charge separation, observing that photocurrent is about 5.5 times greater than pure ZnO.
- Excellent performance in the decomposition of ofloxacin (Ofx) and methylene blue (MB) under visible light illumination and sunlight.
- The role of photoactive species in the reaction process was ordered as follows: $h^+ > HO > e^-$.

1 Introduction

Photocatalysis for advanced oxidation process to treat persistent organic matter in water is one of the prominent topics of research interest [1–3]. ZnO-based materials are still one of the most promising candidates due to their ease of fabrication, low cost, non-toxicity, and biocompatibility. Besides, its superior properties include chemical stability over a wide pH range (pH: 4–9), thermal stability, high optical stability, and a wide radiation absorption band. [3, 4] Interestingly, ZnO absorbs sunlight higher than other metal oxide semiconductors and has more light quanta [5]. For example, ZnO has a wide and straight band gap similar to TiO₂, but the electron mobility of ZnO is 10–100 times higher than that of TiO₂, so the electron transfer efficiency and photocatalytic efficiency of ZnO are higher than TiO₂ [6]. However, like TiO₂ and some other semiconductor oxides, the wide bandgap energy and fast electron-hole pair recombination limit the application of ZnO in reality [1, 7–9]. Therefore, the strategy to reduce the band gap energy and the electron-hole pair recombination rate has been of intense research interest. Doping metal or non-metal into ZnO has proven to be the most simple but highly effective solution [10–12]. The atomic size of non-metallic elements is usually smaller, so doping non-metals into a ZnO crystal lattice is often much easier experimentally than metal doping. On the other hand, the incorporation of metal doping can occasionally result in the creation of vacancies or defect states, which have the potential to act as recombination centers for photogenerated electrons and holes. For the Mn dopant case, when the average distance between the electron traps decreases, the sites where the doped Mn enters will act as photogenerated electron and hole recombination centers, therefore reducing the efficiency of the photooxidation reaction when the amount of doped Mn is more than optimal [13].

The feasibility of doping non-metallic elements through theoretical calculations has been demonstrated by Asahi et al. [14]. Moreover, non-metallic doping such as C, N, and S into ZnO has been demonstrated by W. Yu et al. based on Density Functional Theory (DFT) calculations. The structure-electron and optical properties calculations

suggested that N and C doping in the ZnO lattice is much more efficient than S doping in absorbing more intense light in visible and near-ultraviolet regions. The effective mass calculation of the photogenerated electrons and holes showed that the recommendation rate of pairs electron-hole doping is arranged in the following order: C_{doped} < N_{doped} < S_{doped} [15].

Up until now, there have been a few publications on C-doped ZnO photocatalysts. [16–22] However, studies on C-doped ZnO photocatalysts are still few and abundant in terms of morphology, synthesis methods, and applications. Most of the reports focus on the degradation of dyes such as MB and RhB, [16–20] and the rest on the degradation of other organic substances such as p-aminobenzoic [21] acid or Bisphenol A [22]. Besides, very few reports surveyed the optimal conditions for photocatalysis, and some showed that characteristic studies of C-doped ZnO are not comprehensive [17, 21, 22]. In particular, photoelectrochemical properties are rarely used for research. The studies also showed that the obtained C-doped ZnO has an unimpressive specific surface area and photocatalytic efficiency. For example, most of the C-doped ZnO samples obtained have specific surface areas less than 21 m²/g except for the study of P.M. Perillo et al. (S_{BET} = 33.29 m²/g) [21], and this may be related to their photocatalytic efficiency. In addition, the effect of carbon doping on reducing the band gap energy level, thereby improving ZnO photoabsorption in the visible and ultraviolet regions, was also investigated. However, these reductions were slight, even with the band gaps still in the UV region [22]. Maybe a slight bandgap reduction is related to precursors used as carbon resources or the synthesis methods.

In summary, the above analysis shows that, although there have been studies on carbon-doped ZnO materials, they are not many and comprehensive. Research results mainly focus on the degradation of dyes or other organic substances but have not focused on the degradation of antibiotics in water. Besides, studies on the properties of C-doped ZnO materials are limited, such as photoelectrochemical properties, including electrochemical impedance or photocurrent measurement. Moreover, diversity in morphology, synthesis method, and application of materials has not been found. Therefore, studies on carbon-doped

ZnO materials should still be encouraged to continue further research to enrich and comprehensively view this material.

This work synthesized C-doped ZnO nanoparticles (NPs) by the hydrothermal method using precursor zinc acetate and polyvinyl alcohol (PVA) with different molar ratios of PVA/Zn²⁺. The photo-oxidation performance of C-doped ZnO was also studied based on the degradation of antibiotics (ofloxacin, Ofx) and dyes (methylene blue, MB) under visible light. The influence of doped C content on optical, photoelectrochemical, and photocatalytic properties was investigated and discussed in detail. Furthermore, COD removal and TOC mineralization performance were analyzed. Finally, the radical scavenging test was investigated, and from that, the photo-oxidation reaction mechanism for MB and Ofx was proposed.

2 Experimental

2.1 Materials

Zinc acetate dihydrate (Zn (CH₃COO)₂·2H₂O, 99.5%), ethanol (C₂H₅OH, 99.5%), sodium hydroxide (NaOH, 99%), and polyvinyl alcohol (PVA, 99%) were bought from Sigma Aldrich, USA. Ofloxacin (Ofx, 98%), methylene blue (MB, 99.5%), silver nitrate AgNO₃ (99.8%), ethylenediamine tetraacetic acid (EDTA, >99%), isopropanol (99.5%), and 1,4-benzoquinone (99%) were obtained from Xilong Scientific Co., Ltd., China.

2.2 Preparation of CZ

CZ catalysts were produced via a hydrothermal process with precursors such as zinc acetate and polyvinyl alcohol, sodium hydroxide as the base, ethanol, and deionized water as the solvent. The molar ratio of PVA/Zn²⁺ is 5, 10, and 15%, respectively. The mass of Zn(CH₃COO)₂ salt is 0.664 g, and the mass of PVA is 0.0067; 0.0134, and 0.02 g, respectively. The synthesized samples are denoted CZ1, CZ2, and CZ3, respectively.

First, 0.664 grams of zinc salt are blended with 50 ml of C₂H₅OH, and an appropriate amount of PVA is dissolved in 40 ml of 50 °C deionized water on a magnetic stirrer until completely dissolved, then they are mixed and stirred for 30 min. Next, the solution, which includes 1.2 grams of NaOH in 70 ml of C₂H₅OH, is added gradually while the mixture is stirred for an hour at room temperature. The mixture is placed in an autoclave and stabilized at 160 °C for 20 hours. Then cool the reaction vessel to room temperature. The CZ-NPs powder was gathered after repeated washings in distilled water and ethanol and drying at 85 °C for 8 hours.

2.3 Characterization

The crystal structure of the CZ powder was researched using X-ray diffraction (XRD) on D2 PHASER (Germany), with $\lambda_{\text{CuK}\alpha} = 1.5418 \text{ \AA}$. The Scherrer formula (1) calculates the average crystal size.

$$L = \frac{0.9\lambda}{\Delta(2\theta) \cdot \cos\theta} \quad (1)$$

Where: - L: crystallite size;

- λ : wavelength of radiation, $\lambda = 1.5418 \text{ \AA}$;

- $\Delta(2\theta)$: full width of half maximum.

The equation calculates the lattice parameters of the hexagonal cell.

$$\left(\frac{1}{d_{hkl}}\right)^2 = \left(\frac{h^2 + k^2 + hk}{a^2}\right) + \frac{l^2}{c^2} \quad (2)$$

Where d is the distance between planes with the provided Miller indices of h, k, and l, and a, b, and c are the constants of the lattice.

The morphology and chemical composition of catalysts were studied on (FE-SEM) using an S-4800 device (HITACHI, Japan) combined with EDX. The content of carbon in C-ZnO by means of CHNS analysis on a Thermo Fisher Flash SMART (2018) device, Germany. The surface chemical state of the samples was inferred using a PHI X-ray photoelectronic device (PHI Quantera SXM, Japan). UV-Vis measurement was done in the range of 250–800 nm on diffuse reflectance spectroscopy (V-500 Jasco, Japan). The functional groups' analysis was characterized by FT-IR spectroscopy using a 55 Equinox Bruker (Germany). Specific surface areas of the prepared products were measured by the Quantachrome Autosorb IQMP/XR instrument. The BET and BJH methods calculated the specific surface areas and the mesoporous distributions. The photoelectrochemical properties of the catalyst sample (photocurrent and EIS spectra) were measured by BioLogic SP-240. The catalyst sample was dropped on an FTO transparent conductive film as a working electrode. The counter and reference electrodes were Pt wire and Ag/AgCl (3 M KCl), respectively. The electrolyte was 0.1 M Na₂SO₄ in a three-electrode system under a Philips 150 W halogen lamp. Inductively coupled plasma-optical emission spectrometry (ICP-OES) measurement was used to detect the leaching of the ion Zn leaching.

2.4 Photocatalytic investigate

The present study examined the photocatalytic efficacy of CZ powder when exposed to visible light, as determined by its ability to degrade MB and Ofx. The visible light source

was a 150 W Philip halogen lamp (HL, 100 mW/cm²) with a 390 nm UV-cut filter.

In a typical test, a reaction mixture consisting of 100 ml of 10 mg/L MB or 15 mg/L Ofx solution and 0.05 g of CZ catalyst. The solution was shaken in the absence of light for 90 minutes until it attained adsorption equilibrium. Subsequently, extract 4 ml of the solution and centrifuge it for the gathered catalyst. Following this, determine the optical density of the resulting solution at time zero (A₀). Next, turn on the HL and keep stirring. Every 30 minutes, 4 ml of the suspension was removed from the solids and measured for optical density (A_t). The experiment was carried out until the MB solution was completely decolorized. MB concentration was determined on a UV-Vis instrument (Evolution 600, Thermo Fisher, USA) with 200 to 800 nm wavelengths.

The MB decolorized efficiency (H, %) is calculated using the following formula:

$$H(\%) = \frac{C_o - C_t}{C_o} \times 100 = \frac{A_o - A_t}{A_o} \times 100 \quad (3)$$

A_t and A₀ were identified as the peak values at wavelengths of 665 nm (MB) and 288 nm (Ofx) at time $t = 0$ and t min, respectively. The C_o and C_t (mg/L) represent the concentration of MB at time $t = 0$ and t min, respectively. The kinetics of the MB decomposition reaction (with a small MB concentration) fit the pseudo-first-order kinetic model, so the reaction rate constant (k_{app}, min⁻¹) is calculated by the following equation [4]:

$$\ln\left(\frac{C_o}{C_t}\right) = \ln\left(\frac{A_o}{A_t}\right) = k_{app} \cdot t \quad (4)$$

The photocatalytic efficiency was evaluated based on chemical oxygen demand (COD) [23, 24], determined according to SMEWW 5220D:2017 for wastewater investigation and total organic carbon (TOC) mineralization efficiency, using a Shimadzu TOC-VCPH analyzer (Japan), as expressed in Eqs. (5) and (6), respectively:

$$\text{COD removal efficiency}(\%) = \frac{[\text{COD}]_o - [\text{COD}]_t}{[\text{COD}]_o} \times 100 \quad (5)$$

$$\text{TOC mineralization efficiency}(\%) = \frac{[\text{TOC}]_o - [\text{TOC}]_t}{[\text{TOC}]_o} \times 100 \quad (6)$$

The role of photo-oxidation pieces in dye solution decomposition was studied by adding some agents such as ethylene diamine tetra acetic acid (1 mM, EDTA-2Na, catch h⁺), 1,4-benzoquinone (1 mM, p-BQ, catch ·O₂⁻), isopropanol (1 mM, isop, catch ·OH), and silver nitrate (1 mM, AgNO₃, catch e⁻) into the solution before turning on the light.

3 Results and discussion

3.1 XRD, FT-IR, Raman, and UV-Vis -DRS

The X-ray diffraction method investigated the structural and crystal phase composition of C-doped ZnO catalysts. XRD results (Fig. 1a) showed that CZ1, CZ2, and CZ3 materials all have a single-phase-hexagonal wurtzite structure that resembles pure ZnO, with lattice plane families (100), (002), (101), (102), (110), (103), (200), and (112) (JCPDS 00-036-1451). The sharp, high diffraction peaks confirmed that the hydrothermal process, combined with calcination, formed C-doped ZnO nanoparticles with high crystallinity. The XRD pattern does not present phases of C and its compounds or other impurities. However, close observation shows that the positions of the diffraction peaks of the CZ1, CZ2, and CZ3 slightly shift towards the two theta angles smaller than those of the pure ZnO. That indicates carbons (from PVA and ethanol sources) are doped into the ZnO lattice during hydrothermal and calcination processes, entering the lattice defects or partially displacing the O or Zn locations without altering the structure of ZnO. The same result was found in the report of O. Bechambi et al. [22].

The average crystallite size and lattice constant of catalysts were calculated from the XRD data. Table 1 shows that the crystallite sizes of CZ1, CZ2, and CZ3 are not significantly different compared with the undoped ZnO. Notably, the lattice constants of CZ differ slightly in comparison to those of undoped ZnO. However, the *c/a* ratio of the doped and undoped ZnO materials is approximately ~1.6. In short, C-doping changes the lattice constant and the position of diffraction peaks in ZnO materials.

The bonding properties of the materials were studied using the FT-IR infrared spectroscopy method. Infrared spectroscopy results (Fig. 1b) show the peaks at wavenumbers 3430 and 1630 cm⁻¹, which confirmed typical O-H bond oscillations due to water surface adsorption [22]. The spectral region between 400–600 cm⁻¹ was utilized to detect the metal-oxygen bonds, with the Zn-O bond exhibiting a peak at 432 cm⁻¹. The other peaks were at a higher wavenumber for the C-doped ZnO. The above results are explained: oxygen was replaced by carbon (C_o) at their positions, which will impact the mass and strength of the chemical vibration, thereby affecting the absorption peak position. The decreasing mass in the bond was related to the lower molecular weight of the Zn-C vibration in comparison to the Zn-O vibration. Next, the additional appearance of a covalent Zn-C bond beside the ionic Zn-O bond in the crystal lattice is required by the significantly lower electronegativity of C (2.55) compared with O (3.44). The Zn-C bond increases as the amount of C_o increases, which again implies a shift towards some higher waves. Moreover, the

Fig. 1 **a** XRD diffraction patterns, **b** FTIR spectra; and **c** Raman spectra of ZnO, CZ1, CZ2, and CZ3

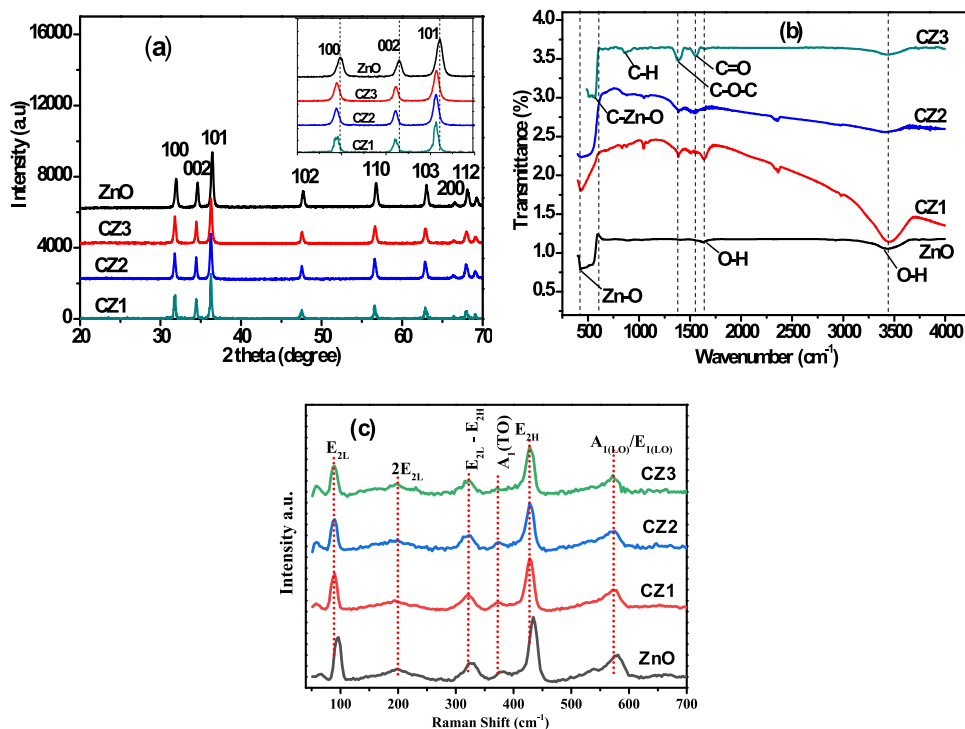


Table 1 Lattice parameters and average crystallite size of CZ1, CZ2, CZ3, and undoped ZnO

Materials	L (nm)	a, b (Å)	c (Å)	c/a
ZnO	32.0	3.2505	5.2004	1.6000
CZ1	32.5	3.2492	5.2068	1.6025
CZ2	31.7	3.2512	5.2050	1.6001
CZ3	31.3	3.2527	5.2067	1.6001

influence of the C dopant is shown by the description of weak peaks at 860, 1398, and 1570 cm^{-1} , respectively, referred to as the C-H, C-O, and -C = O bonds [25, 26].

The bond characteristic of the obtained catalysts was further clarified by the Raman spectra of pure ZnO and CZ particles, which were displayed in Fig. 1c in the 10 cm^{-1} – 700 cm^{-1} . The results revealed a prominent and narrow peak at 437 cm^{-1} , which was assignable to the E_{2H} mode of zinc oxide. This observation indicates the presence of a characteristic feature of wurtzite ZnO with a high degree of crystallinity [27, 28]. The E_{2L} mode can be attributed to the peak observed at 98 cm^{-1} , which is a shared performance of both pure ZnO and CZ powder. Besides, two peaks of $2E_{2L}$ and second-order scattering $E_{2H}-E_{2L}$ were recorded at 209 and 334 cm^{-1} , respectively [22]. The incorporation of impurities and defects in C-doped samples leads to a significant reduction in the intensity and shift to a lower wave number of Raman peaks, owing to the disruption of translating crystal symmetry [28]. The replacement of oxygen (O) by carbon (C) leads to the formation of oxygen

vacancies (V_o) and/or C-Zn-C and C-Zn-O bonds, which could explain an increased disorder of ZnO structure, in obedience to the gradual reduction of the oxygen content in the compound [29]. Additionally, the polar mode of $A_{1(LO)}/E_{1(LO)}$ has been demonstrated at approximately 570 cm^{-1} for C-doping. The representation of scattering contributions obtained outside the Brillouin zone center is indicative of the shifting and broadening of phonon modes. The phonon mode $A_{1(LO)}/E_{1(LO)}$ is commonly depicted through the defect complexes formed by the zinc interstitial and V_o in the ZnO lattice [28]. The Raman results agree with the X-ray diffraction (XRD) and FTIR investigation.

C doping in ZnO was further clarified in the results of UV-Vis-DRS spectral analysis (Fig. 2). The results illustrate the higher optical absorption value of CZ catalysts than pure ZnO in the UV and Vis regions. The increased absorption of the UV region is a favorable factor for the photocatalytic reaction when the radiation source is UV light or sunlight. In addition, the absorption edges of CZ materials with a redshift are also observed, corresponding to the extension of visible light absorption and decreasing bandgap energy (Table 2). Similar results were also found in the reports of A. S. Alshammari et al., O. Haibo et al., and S. Liu et al. [16–18] In this study, the bandgap energies of CZ1, CZ2, CZ3, and pure ZnO (Fig. 2b) are 2.86, 2.77, 2.79, and 3.10, respectively. The ZnO band gap energy decreased significantly (0.24 eV) when carbon doped in the presence of 5% mole of PVA during the process, continued to decline slightly (0.07 eV) when increasing the PVA content to 10%

Fig. 2 a UV-Vis-DRS spectra, b band gap of ZnO, CZ1, CZ2, and CZ3

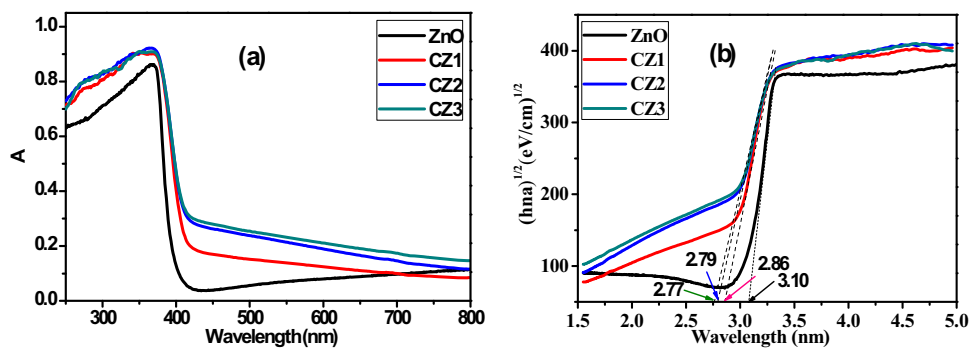


Table 2 The E_g and λ of the CZ1, CZ2, CZ3, and pure ZnO

Materials	h (j.s)	C (m/s)	E_g (eV)	λ (nm)
ZnO	$6.626 \cdot 10^{-34}$	$3 \cdot 10^8$	3.10	400
C-ZnO1	$6.626 \cdot 10^{-34}$	$3 \cdot 10^8$	2.86	434
C-ZnO2	$6.626 \cdot 10^{-34}$	$3 \cdot 10^8$	2.79	445
C-ZnO3	$6.626 \cdot 10^{-34}$	$3 \cdot 10^8$	2.77	448

(1 eV = $1.602177 \cdot 10^{-19}$ J; 1 m = 10^9 nm)

mole, and decreased insignificantly (0.02 eV) with increasing PVA by 15% mass. It was noticed that when increasing the molar ratio of PVA/ Zn^{2+} from 10 to 15%, the band gap energy decreased insignificantly (0.02 eV). Thus, it can be considered that with a molar ratio of 15%, carbons replace the oxygen sites in the lattice at almost the maximum. The CZ3 bandgap has the most reduction, with $E_{gCZ2} = 2.77$ eV relating to the optical absorption wavelength with $\lambda \leq 448$ nm. Found that C-doped ZnO nanoparticles obtained in this work by the hydrothermal method with PVA, ethanol, and acetate as carbon sources have a more significant band gap energy reduction (0.33 eV) than in other works, for example, the carbon source from pluronic F127 (0.19 eV) [18], or polyethylene glycol (PEG) and urea (0.16–0.23 eV) [16], or carbon graphite and acetic acid (0.1 eV) [22].

According to research by W. Yu et al. [15], The VB of ZnO mainly comprises O2p and Zn 3d states and only a little of Zn 3p states. The CB of ZnO primarily consisted of Zn 3p and Zn 4s orbitals with roughly equal contributions, interspersed with a few O2s states. The Fermi level of pure ZnO is mainly the O2p state. During the reaction, the C2p state of the doped carbon will approach the Fermi level of ZnO due to the similarity in atomic size and electronegativity with oxygen atoms. Doping carbon into ZnO by substituting oxygen sites is considered p-type doping because carbon has fewer valence electrons and less electronegativity than oxygen. The substitution of oxygen sites in the doped carbon, which forms vacancies at a slightly higher level than the Fermi level, thus modifies its electronic configuration in proximity. As a result, Fermi-level electrons can quickly jump into higher energy regions using

these defects formed through thermal or optical excitation. Moreover, further widening the valence band by generating vacancies can close the band gap and produce a wider light absorption band. In short, changes in the electronic configuration near the Fermi level can significantly affect the physical properties and photocatalytic activity of semiconductors [15].

3.1.1 SEM results

The SEM image (Fig. 3) shows that the particles in the undoped ZnO sample have many different morphologies, including spherical-like nanoparticles, flat plates of different sizes, and a few large-sized long bars. For PVA/ $Zn^{2+} = 5\%$ mole, the morphology of the catalyst is somewhat improved, with the particles gradually becoming more sharp and uniform. However, the particles still exist in many different shapes and sizes. When increasing the PVA content to 10–15%, corresponding to the increased carbon doping (sample CZ2, CZ3), the particles become uniform in shape, clear, and sharp. Notably, the cross-section of particles has a unique hexagonal shape. However, the sample CZ2 particles are not uniform in size and are still clustered Fig. 3c. This limitation is improved when the PVA content is increased to 15%. Interestingly, the particles no longer aggregated, becoming more uniform in size, where the length is about 40–200 nm, the width is about 40–100 nm, and the height is about 30–50 nm. The result is similar to the XRD and UV-Vis results, where the crystal size and band gap energy are nearly equal.

3.1.2 Photoelectrochemical performance

To evaluate the effect of doping C into ZnO on interfacial charge carrier separation, the arc radius of Nyquist plots was used to consider a greater probability of separating photoexcited electron-hole pairs, a charge transfer, and an interfacial charge transfer resistance at the surface of the catalyst [30]. Upon exposure to visible light, it has been noticed that the C-doped ZnO rod arc radius is comparatively smaller than that of pure ZnO (Fig. 4a), suggesting

Fig. 3 SEM images of **a** ZnO, **b** CZ1, **c** CZ2, **d** CZ3 on a scale of 500 nm, and **e**, **f** CZ2 and CZ3 on a scale of 200 nm

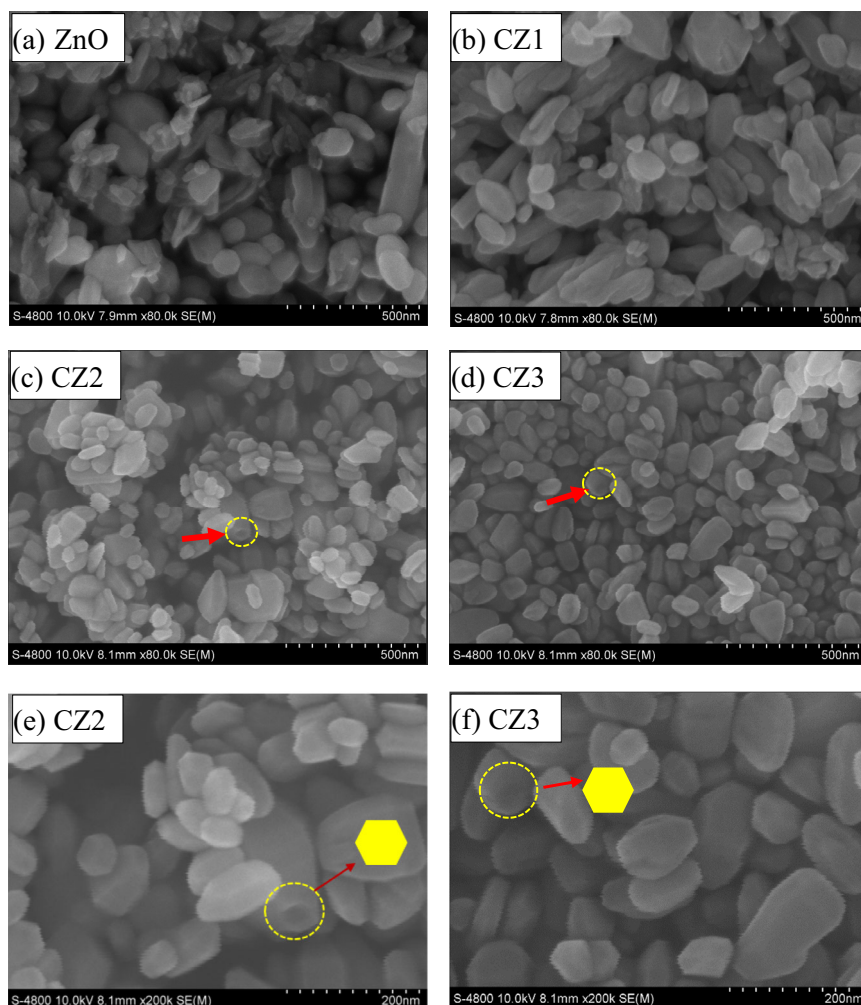
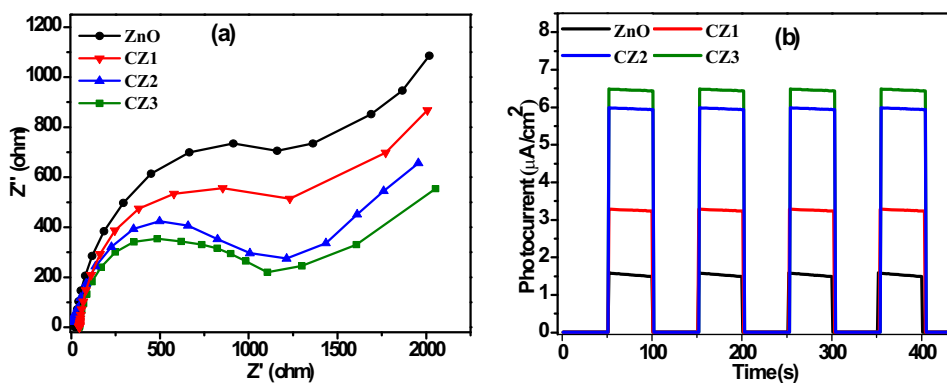


Fig. 4 **a** Nyquist EIS plots and **b** Photocurrent response of ZnO, CZ1, CZ2, and CZ3



that the former exhibits lower electrochemical resistance compared to the latter, and has a more pronounced interfacial charge transfer. In our study, we found that the relative arc radius followed the order of $CZ3 < CZ2 < CZ1 < ZnO$. The decreased band gap of CZ nanoparticles compared with ZnO pure will help improve the electron-hole pairs (under visible light) at the photocatalyst surface. Besides, the formation of trap sites from C-doping in the

ZnO band structure also increases the lifetimes of the excited electrons of the CB [31, 32]. This phenomenon can be accounted for by the accelerated inter-surface charge transfer and enhanced separation of photocarriers. The incorporation of doping carbon results in an improvement in the moving capacity of photocarriers when under the influence of light in the visible spectrum, which has the potential to increase the photocatalytic performance of CZ.

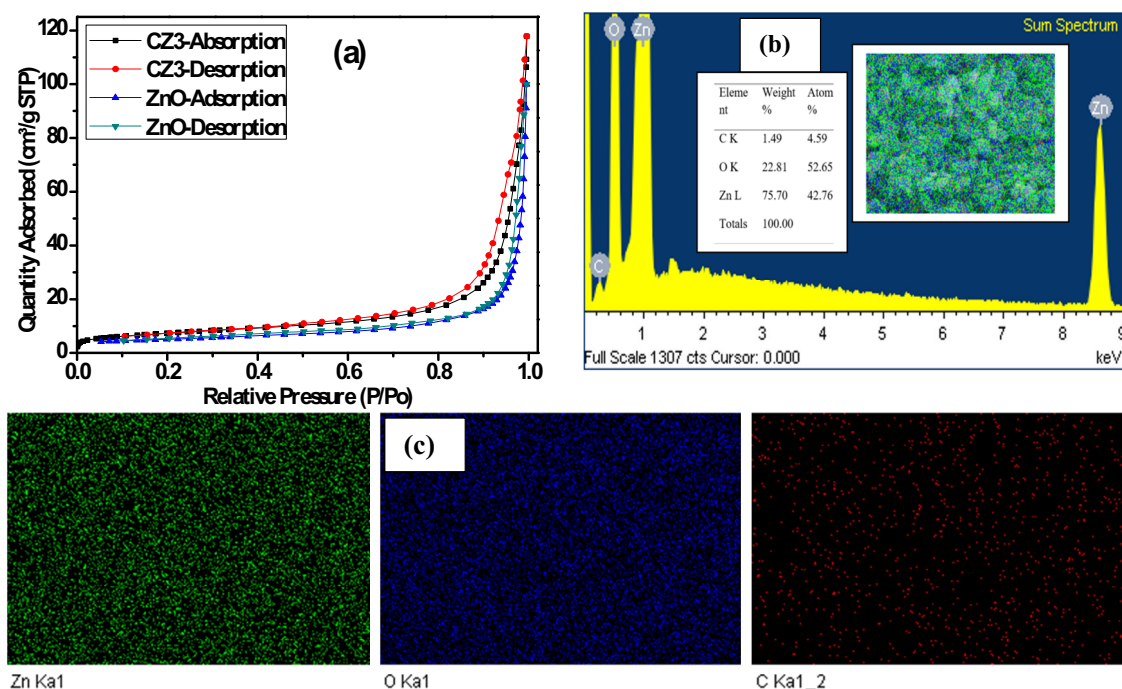


Fig. 5 a the N₂ adsorption-desorption isotherms of CZ3 b EDX of the CZ3, c scanning elemental mapping

The current-time (J-t) graph at 0 V vs Ag/AgCl has been used to investigate individual photoresponses of the catalyst (Fig. 4b). It has been discovered that after the impurity C level is formed in band gap ZnO, the photoresponse of the catalyst significantly improves. The stable and highest saturation photocurrent density is 6.4 $\mu\text{A}\cdot\text{cm}^2$ for the self-biased CZ3 catalyst, 4.15 times higher than pure ZnO (1.54 $\mu\text{A}\cdot\text{cm}^2$). The observed increase in photocurrent can be attributed to the reduced band gap of the C-doped nanoparticles, leading to enhanced absorption of visible light. The observed trend in the photocurrent density of the photocatalysts, as a function of the amount of C, indicates a notable enhancement in the efficiency of charge separation. A photocurrent spike was shown in Fig. 4b immediately after sun illumination in the chronoamperometry measurement of all the catalysts, demonstrating the immediate formation and separation of electron-hole pairs and providing a high photogenerated carrier density to the catalysts.

3.1.3 EDS and BET results

The photodegradation of the MB activity proceeds on the surface of catalysts, hence surface area serves as essential in ensuring that there is adequate space and surface for the catalyst to interact with the MB. Therefore, the N₂ adsorption-desorption isotherms were measured in the surface areas of catalysts (Fig. 5a). The results show that the N₂ desorption isotherm belongs to type IV according to the BJH classification. The CZ3 has a specific surface area of 26.04

m²/g, a total adsorption pore volume of 0.155 cm³/g, and a total desorption pore volume of 0.185 cm³/g, which is higher than the undoped ZnO with a specific surface area of 17.6 m²/g, a total adsorption pore volume of 0.155 cm³/g, and a total desorption pore volume of 0.185 cm³/g. This clearly shows that the surface area of CZ3 is 1.4 times higher than that of ZnO. It may be due to the CZ3 nanoparticle having i) smaller, ii) unaggregated particles, and iii) more uniform particle shapes than those of the undoped ZnO, as shown in the SEM figure. The specific surface area of the CZ3 nanoparticle in this report is higher than that of the C-doped ZnO materials reported by A. S. Alshammari (17.10 m²/g), [18] by O. Bechambi (15.00–21.00 m²/g) [22], and close to the results of S. Liu (4.00–27.60 m²/g) [16].

EDS results (Fig. 5b) show the existence of peaks characteristic for elements C, O, and Zn with the respective mass percentages of 1.49 wt. %, 22.81 wt. %, and 75.70 wt. %. The C content of CZ3 determined by the EDS is 1.49 wt. % and by CHNS analysis is 1.34 wt. %. The mass percentage of C doped is relatively small because the synthesis process involves heating the product after the hydrothermal process at 300 °C for 2 hours. This process removed the doped C from the surface of materials and helped the doped C penetrate and bind better in the ZnO lattice. In addition, the EDS mapping (Fig. 5c) results provide a visual image of the even distribution of the elements C, O, and Zn in the sample. In addition to these elements, there are no other foreign elements, proving that the synthesized CZ material has high purity.

3.1.4 XPS results

The surface chemistry of the CZ3 nanoparticles was analyzed using XPS spectroscopy. Figure 6a shows the binding energy of Zn 2p, O1s, and C1s peaks. The chemical state of Zn in the Zn-O bond is +2 because it is determined by the position Zn2p_{3/2} (1022.1 eV), Zn2p_{1/2} (1045.2 eV) and the distance between the two Zn2p orbitals 23.1 eV, as shown in Fig. 6a' [33]. The present study reveals a blue shift (0.2 eV) in the Zn2p_{3/2} and Zn2p_{5/2} of CZ3 nanoparticles in comparison to pure ZnO. This is because C-dopant and Ovac typically result in a blue shift of the Zn-O bond. Furthermore, it was observed that Zn2p_{3/2} of the CZ3 nanoparticles can be resolved into three component peaks (as depicted in Fig. 6a'). These peaks correspond to Zn-O-C/Zn-C (1020.9 eV), Zn-O (1021.7 eV), and Zn-Ovac (1022.5 eV) [18]. A large peak O1s (Fig. 6b) located at 530.1 eV in pure ZnO is Zn bonds with O²⁻ in the wurtzite ZnO lattice [32], while the shoulder peak (531.6 eV) is the OH- group or carbonates [34]. The peak observed at 530.2 eV in the CZ2 nanoparticles is a property of O²⁻ ions, while the peak observed at 529.6 eV can likely be assigned to Zn-Ovac and Zn-O-C bonds. The remaining peak at 532.7 relates to characterizing C-O and C=O bonds [34–36]. At the same time, a broad peak C1 (Fig. 6c) for the CZ3 particles, involving the deconvolution peak at 284.5 eV, 286.2 eV, and 288.58 eV. These peaks indicate the C-C, Zn-O-C/Zn-C, and C=O bonds, as reported in the references [36–38]. Besides, the asymmetric C1s peak of the CZ3 nanoparticles has a 0.2 eV blue shift compared to pure ZnO (284.7 eV) because the negatively charged O_{vac} would transfer more electron density onto C. The photocatalyst's energy levels are influenced by diverse Zn-C species, thus affecting both the E_g and the optical absorption wavelength.

3.1.5 Photocatalytic test results

The influence of doped C content on the photooxidation activity of ZnO was investigated via the degradation reactions of MB and Ofx under visible light, as shown in Fig. 7.

Figure 7a shows the decrease of MB concentration over time in the presence of catalysts and visible light irradiation. It was found that the decrease in MB concentration occurred in the order ZnO < CZ1 < CZ2 ~ CZ3. The reaction rate constants of ZnO, CZ1, CZ2, and CZ3 (Fig. 7b) are 0.0158; 0.0197; 0.0291, and 0.0334 min⁻¹, respectively, while the reaction rate constants of CZ1, CZ2, and CZ3 are 1.25, 1.82, and 2.10 times those of ZnO, respectively. For the Ofx decomposition reaction (Fig. 7b), a concentration decrease was quite similar to the MB degradation reaction. Specifically, the reaction rate constants of ZnO, CZ1, CZ2, and CZ3 are 0.0067, respectively; 0.0107; 0.0134, and

0.0148 min⁻¹, where the reaction rate constants of CZ1, CZ2, and CZ3 are 1.6, 2.0, and 2.2 times that of ZnO, respectively. Through this, it can be seen that there is a substantial decrease in organic matter concentration when increasing the doped carbon content, corresponding to an increase in the molar ratio of PVA/Zn²⁺ from 5–10%. Meanwhile, a negligible decrease in the organic concentration was observed with a continued increase in doped carbon content, corresponding to an increase in the PVA/Zn²⁺ molar ratio from 10–15%. This result agreed with the UV-vis-DRS and SEM results when the CZ2 and CZ3 samples had similar EG and morphology.

As is known, pH is related to the surface charge of the material, thus affecting the adsorption and desorption of organic substances on the material's surface during the reaction. In this study, solution pH was investigated from 4 to 10 for the MB decomposition reaction and from 4 to 9 for the Ofx decomposition reaction. When not adjusted, the pH of the reactive MB solution is approximately 6.5, and the pH of the Ofx solution is approximately 6.4. The pH of the reaction solution was adjusted with an HCl solution of 0.5 M or a NaOH solution of 0.5 M.

The result of studying the effect of pH on MB degradation from Fig. 8a shows that the degradation of MB is highly efficient in the pH range 4–9, then slightly decreased at pH=10. MB degradation increased slightly in natural or weakly acidic conditions with pH 4–7. The reaction rate constant at pH 4, 5, 6, and 7 was 0.0167; 0.0216; 0.0267, and 0.0354 min⁻¹, respectively. In weak base conditions with pH 8–9, MB degradation increased strongly with reaction rate constants of 0.0564 and 0.0667 min⁻¹, respectively. However, MB degradation decreased slightly when the further pH increased to 10. The isoelectric point (pH_{pzc}) of CZ3 materials was determined to be 7.6. So the material's surface is positive with pH lower pH_{pzc} and vice versa. When pH ≤ 7, both the CZ3 surface and MB are positively charged, so MB⁺ is poorly adsorbed on the CZ3's surface due to repulsive interaction. Therefore, the MB degradation rate is low. In contrast, with pH > 7, the CZ3 surface is negatively charged, so MB adsorption on the CZ3 surface is better, which is favorable for the photooxidative reaction of MB. so that the rate constant increases sharply and reaches its highest at pH = 9 (0.0667 min⁻¹). However, with further increasing pH to 10, the MB degradation efficiency decreases due to a large amount of MB adsorbed on CZ3's surface, causing a light-blocking effect and reducing the quantum efficiency of the photocatalyst process of MB. On the other hand, it is not excluded that the strength of ZnO substrates is affected by the base environment (pH = 10), so MB degradation is slightly reduced.

Solution pH also affects the decomposition of Ofx. The results shown in Fig. 8c show that the Ofx degradation

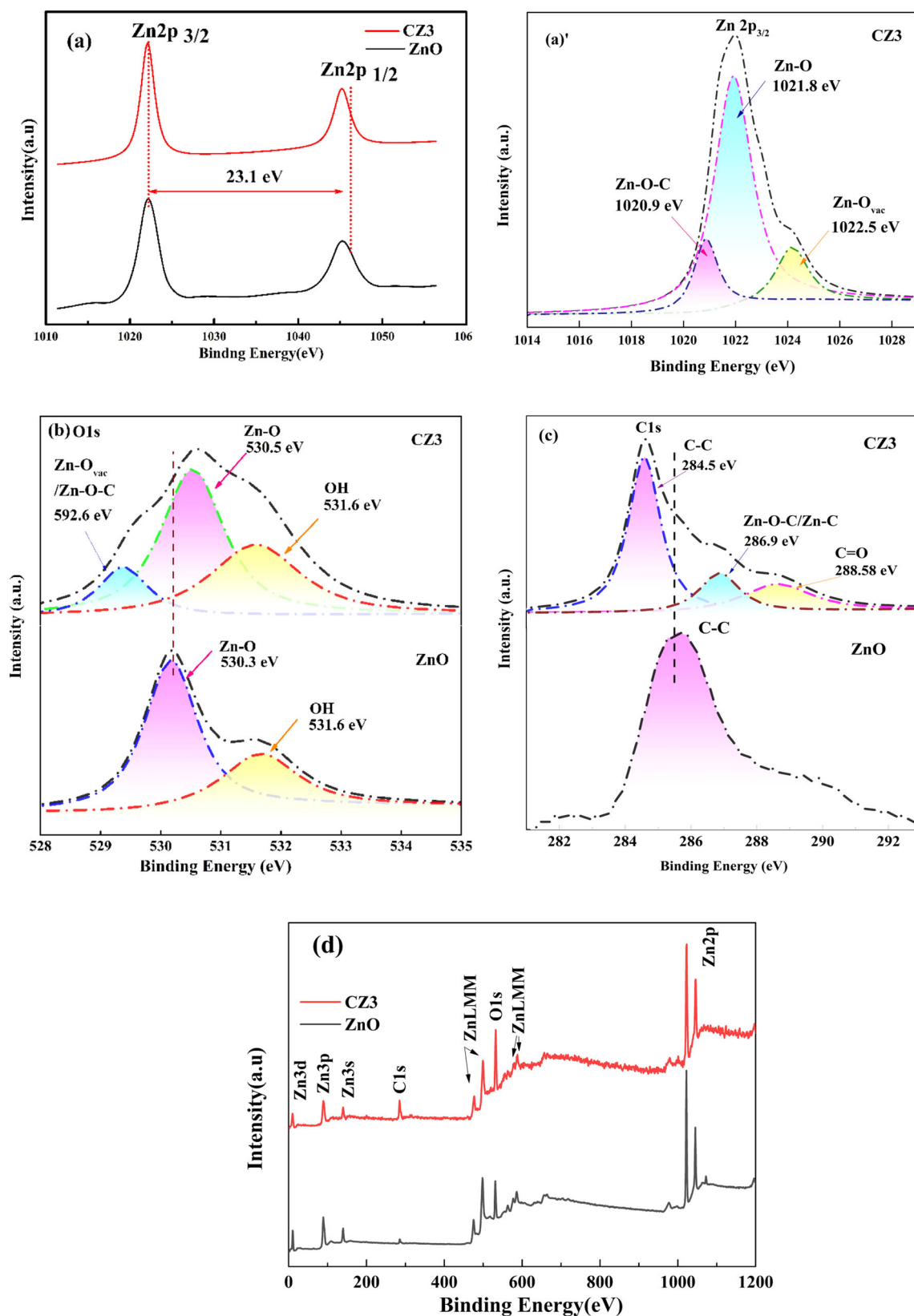


Fig. 6 a Zn 2p and deconvolution, a' Zn 2p_{3/2} b O 1s of CZ3 and ZnO c C 1s high-resolution spectra of ZnO and CZ3 and d full scan spectrum of ZnO and CZ3

Fig. 7 a, c degradation of MB and Ofx concentration versus time; b, d pseudo-first-order kinetic plots of the decomposition of MB and Ofx over the CZ1, CZ2, CZ3, and ZnO catalysts under visible light

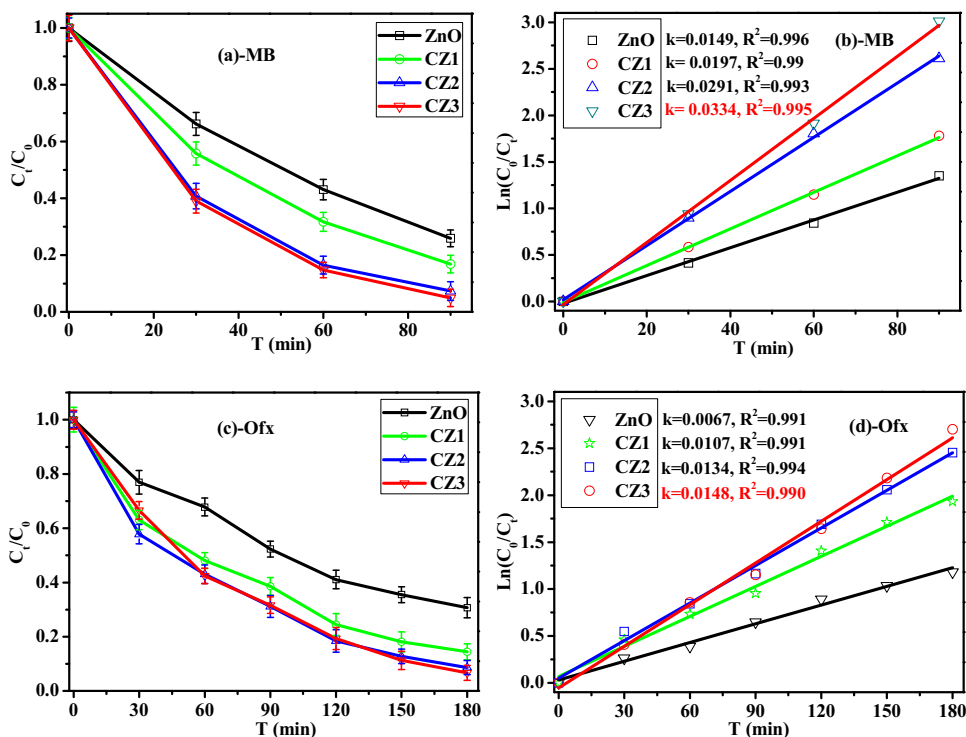
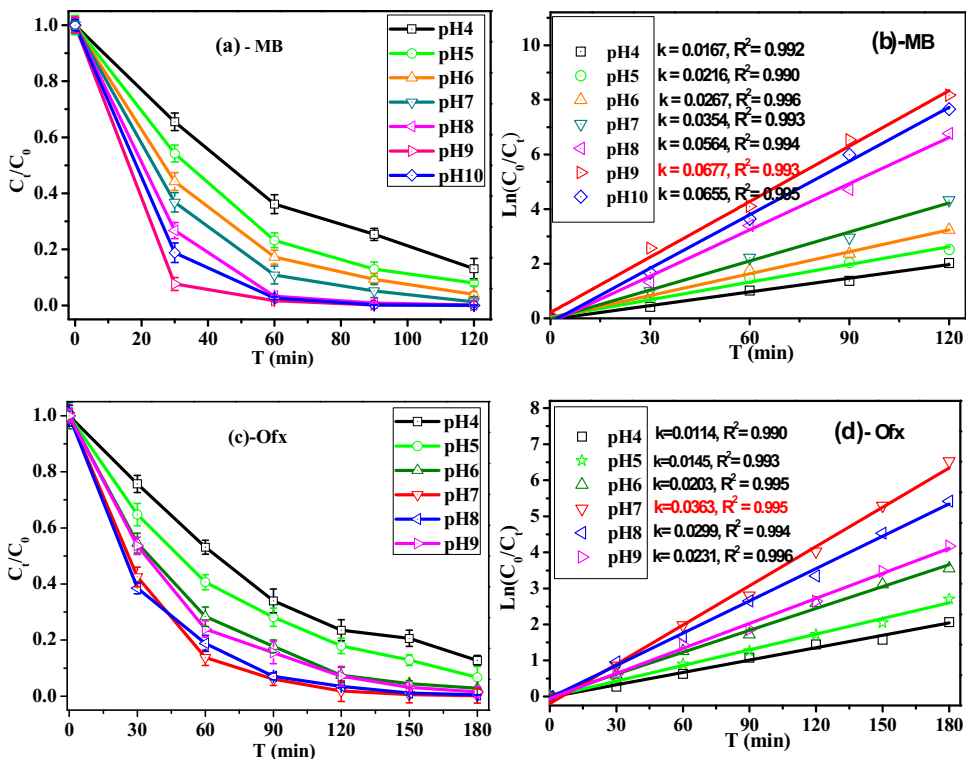


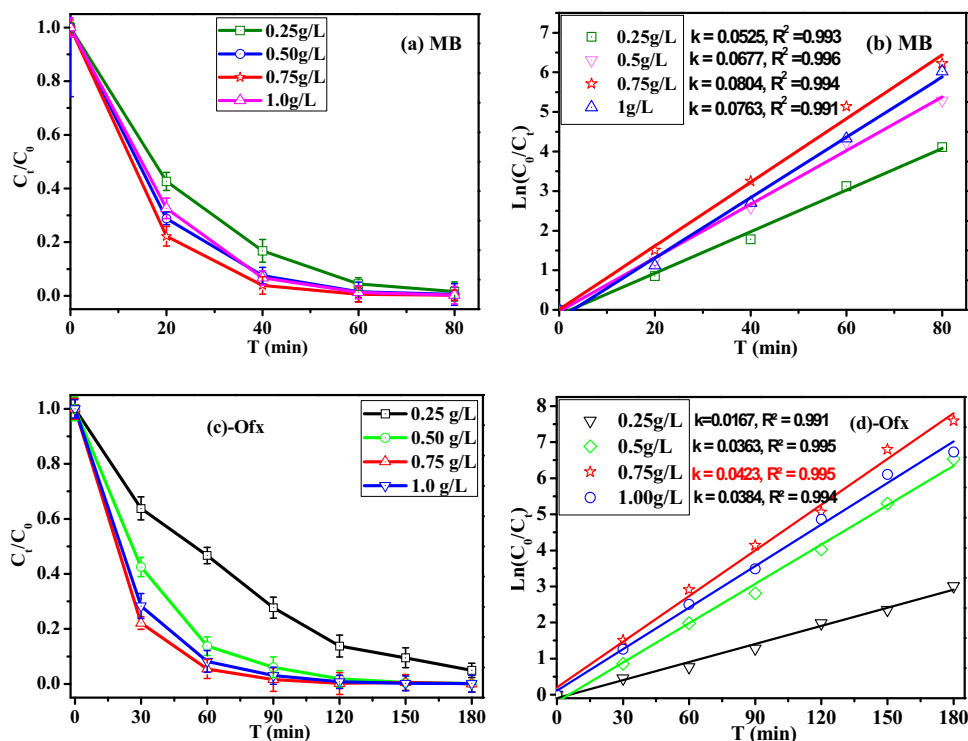
Fig. 8 Degradation of (a) MB and (c) Ofx concentration versus time; pseudo-first-order kinetic plots of the decomposition of (b) MB and (d) Ofx over the CZ1, CZ2, CZ3, and ZnO catalysts under HL or SL



increased slightly from 0.0114 – 0.0203 min⁻¹ in the pH range 4–6 and at pH=9 and increased sharply from 0.0299–0.0363 min⁻¹ in the pH range 7–8. Among them, Ofx decomposition at pH = 7 is the greatest, with a reaction rate constant of 0.0363 min⁻¹, 3.0, and 1.6 times higher

than pH=4 and pH=9, respectively. Acid dissociation constants of Ofx include K_{a1} (6.05–6.10) and K_{a2} (8.22–8.28). Ofx exists in the cationic form (Ofx⁺) below pK_{a1}, the anionic form (Ofx⁻) above pK_{a2}, and the zwitterionic form (Ofx^{+/-}) and the neutral form (Ofx) between

Fig. 9 a, c The effect of catalyst content on the degradation of MB and Ofx and b, d degradation reaction kinetics of MB and Ofx under visible light



pK_{a1} and pK_{a2} . [39, 40] With pH 4–6, both the Ofx and CZ3's surfaces are positively charged, while with pH >8.28, both the Ofx and CZ3's surfaces are negatively charged. This means that both the adsorbent and the adsorbent have the same charge, so they have a repulsive interaction, leading to poorly adsorbed Ofx on the CZ3 surface and a low Ofx decomposition efficiency. With the pH 7–8 range, especially at physiological pH (7.0–7.4), the ratio Ofx^{+/-}/Ofx is the largest, meaning Ofx exists mainly in the form Ofx^{+/-}, and the CZ3's surface is positively charged. Therefore, the adsorption process and Ofx decomposition are enhanced; specifically, the reaction rate constant at pH = 7 is the largest.

In summary, solution pH dramatically affects the efficiency of organic matter decomposition, and the optimal pH is related to the organic nature of the reaction. In this survey, the optimal pH of the MB and Ofx degradation reactions was 9 and 7, respectively.

The effect of catalyst content has also been studied and investigated with an amount of CZ3 catalyst ranging from 0.25 to 1.00 g/L, as presented in Fig. 9. In the presence of a CZ3 catalyst at optimum pH with catalyst content ranging from 0.25 g/L to 0.75 g/L, the degradation rate constants of MB increased from 0.0525 to 0.0804 min^{-1} and of Ofx increased from 0.0167 to 0.0363 min^{-1} . This increase corresponds to an increase in the active sites of the catalyst in the solution. However, with a further rise in catalyst dosage to 1 g/L, the rate constant decreased to

0.0763 and 0.0384 min^{-1} for MB and Ofx, respectively. This decrease is attributed to the overload of the catalyst, which causes mutual shielding and the opacity effect, reducing quantum efficiency and the reaction rate. In short, these results show a similar effect of catalyst content on MB and Ofx degradation efficiency. The efficiency of organic matter decomposition increased with increasing catalyst content from 0.25 g/L to 0.75 g/L, decreasing with increasing catalyst content to 1.00 g/L. Thus, the optimal catalyst dosage within the reaction investigation limit is 0.75 g/L.

The stability of the catalyst has been tested through four uses; the result of Fig. 10 shows a slight decrease in photodecomposition efficiency after each reuse, but the MB or Ofx degradation efficiency is still over 90% after using the catalyst four times. Thus, it can be seen that CZ3 material has high chemical stability and reusability. Besides, the concentration of Zn ion leaching was found 0.144 mg/L in the solution after four cycles.

Also, the ability of CZ3 to do photocatalysis was tested by figuring out how well MB and Ofx removed COD and turned TOC into minerals under the best experimental conditions. Table 3 results show that the COD and TOC values of MB and Ofx decreased significantly after 90 min and 180 min of illumination, respectively. The COD removal efficiency of MB and Ofx was 86.24 and 78.10%, respectively, while the TOC mineralization efficiency of MB and Ofx was 78.57 and 65.98%, respectively. It found

Fig. 10 Reusability of C-ZnO materials for MB (a) and Ofx (b) photodegradation after 80 mins and 180 min irradiated

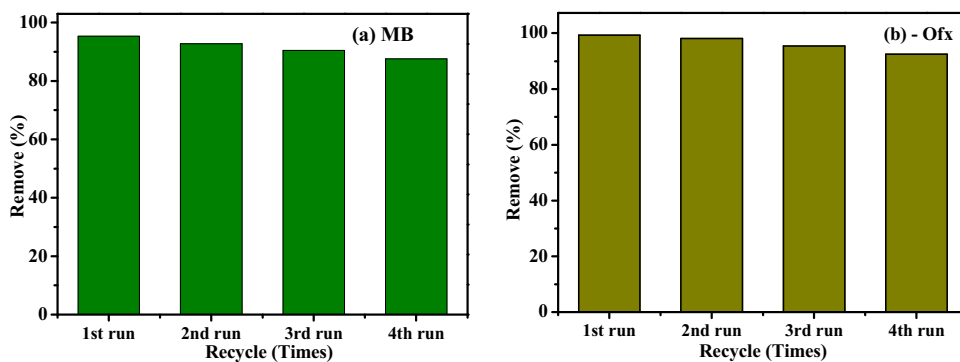


Table 3 The COD removal and TOC mineralize efficiency of MB and Ofx under visible light of CZ3 photocatalyst

Organic	COD (80 mins irradiated)			TOC (180 mins irradiated)		
	Initial (mg.L ⁻¹)	Final (mg.L ⁻¹)	H (%)	Initial (mg.L ⁻¹)	Final (mg.L ⁻¹)	H (%)
MB	51.60	7.10	86.24%	8.40	1.80	78.57%
Ofx	24.20	5.30	78.10%	9.70	3.30	65.98%

that the ability to remove COD from organic substances was more significant than the efficiency of TOC mineralization, suggesting that some intermediate compounds formed during the decomposition of MB and Ofx were inefficiently determined by the COD method. Besides, COD removal and TOC mineralization in MB were significantly higher than in Ofx, possibly because the intermediate products of Ofx degradation progress were more stable. The results of COD removal and TOC mineralization efficiency of MB and Ofx proved that the molecular structure of MB and Ofx was destroyed into organic compounds with smaller structures, and 78.57% of MB and 65.98% of Ofx were completely converted to simple inorganic substances (CO₂, H₂O, etc.).

In general, carbon impurities will cause defects by increasing the surface area, narrowing the band gap, improving photoelectrochemical performance, and increasing visible light-mediated photocatalysis. The effect of carbon impurities and defects has explained the formation of interfacial carbon electron states that bond chemically to ZnO in the band gap, as have the various interactions between carbon and ZnO, as well as the corresponding oxygen vacancies, as mentioned by Sawant et al. [41]. Consequently, the photoinduced carriers exhibit sufficient time to generate oxidizing and reducing agents, which can be effectively employed for the degradation of MB and Ofx, thereby enhancing the photocatalytic efficacy and photoelectrochemical efficiency. Compared with C-ZnO materials in previous studies (Table 4), it shows that the C-ZnO catalyst (CZ3) of this study has a large specific surface area (26.04 g/m²). Therefore, it helps to quickly decompose MB and Ofx under the visible light of a small power lamp (150 W).

To better understand the reaction mechanism and the function of active species such as HO·, h⁺, O₂⁻, and e⁻, trapping agents such as isopropanol (trapping HO·), EDTA-2Na (trapping h⁺), p-benzoquinone (catch (O₂⁻)) and AgNO₃ (capture e⁻) was added during the reaction.[42–44] The results (Fig. 11) showed that the degradation efficiency of MB and Ofx decreased in the presence of radical scavengers. Specifically, with the presence of radical scavengers such as isopropanol, EDTA-2Na, p-BQ, and AgNO₃, the MB degradation efficiency after 90 min was 9.15%, 14.33%, 76.03%, and 38.78%, respectively, while the decomposition efficiency of MB degradation reached 95.30% without radical scavengers being added. Ofx decomposition with the addition of capture agents also obtained similar results. The degradation efficiency of Ofx after 180 min was 16.58%, 20.25%, 85.67%, and 37.40%, respectively, while it was 99.76% in the absence of capturer. The degradation efficiency of the organic remained above 75% with the addition of p-BQ but significantly reduced with the addition of AgNO₃ (<40%) and especially strongly with the addition of isopropanol or EDTA-2Na (<20%). This shows that the contribution of photooxidation pieces to organic matter decomposition is HO·, h⁺, and e⁻, in which HO· and h⁺ are the decisive factors.

The photocatalytic reaction mechanism of semiconductor materials involves the movement of photogenerated electron and hole pairs and the localized position of conduction (CB) and valence (VB) bands. The positions of CB and VB are calculated according to the following formula [45]:

$$E_{VB} = \chi - E^c + 0.5E_g \quad (7)$$

$$E_{CB} = E_{VB} - E_g \quad (8)$$

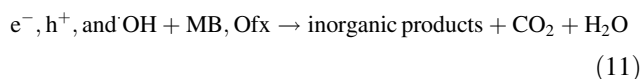
Table 4 The S_{BET} and photodegradation of some organic using C-doped ZnO synthesized by different methods and precursors

Catalyst	Precursors/method	BET (m^2/g)	Organic	Light irradiated	Catalytic dose ($g.L^{-1}$)	k ($min^{-1}/H\%$ (TOC))	Ref.
C-ZnO	Zn(NO ₃) ₂ , PEG, Ure/hydrothermal	12.50	RhB/10 ⁻³ M	Vis, Xenon lamp 350 W	5.00	0.0060	[16]
C-ZnO	Zn(NO ₃) ₂ , Pluronic F127 copolymer/Combustion	17.10	MB/10 ppm	Vis, Xenon lamp 300 W	1.00	0.0060 min ⁻¹	[18]
C-ZnO	Zn(NO ₃) ₂ , melamine/calcination	9.43	RhB 5 ppm	Vis	0.25	0.0088	[19]
C-ZnO	Zn(CH ₃ COO) ₂ /simple precipitation	33.29	PABA 50 μ M	Sunlight	0.50	0.0280	[21]
C-ZnO	Zn(CH ₃ COO) ₂ , C/Hydrothermal	21.00	BPA 50 ppm, H ₂ O ₂ 5.10 ⁻³ M	UV (30 W)	1.00	0.0101/70.00	[22]
C- ZnO	Zn(CH ₃ COO) ₂ , PVA/hydrothermal	26.04	MB 10 ppm Ofx 15 ppm	Vis (HL 150 W)	0.75	0.0804/78.57 0.0363/65.98	This work

RhB Rhodamine B, PABA p-aminobenzoic acid, BPA Bis phenol A

Where: E^c is the free electron energy on the hydrogen electrode scale (4.50 eV), E_{CB} and E_{VB} are the conduction band energy and the valence band energy, E_g is the band gap energy of CZ3, χ is the electronegativity of ZnO in Mulliken ($\chi_{ZnO} = (\chi_{Zn} * \chi_O)^{1/2} = 5.76 eV$). The CZ3 band gap value is 2.77 eV as received from UV-Vis spectra, so the energy values E_{VB} and E_{CB} of CZ3 are 2.645 eV and $-0.125 eV$, respectively.

The suggested mechanism of the reaction is shown in Fig. 12. When irradiating the appropriate light, the electron in the VB of CZ3 gains energy ($h\nu$), then jumps to the CB and creates a hole in the VB. The photogenerated electron (e^-) has a reduced capacity of $+0.50$ to -1.50 V, and the photogenerated hole has an oxidizing capacity of $+1.0$ to $+3.5$ V [3]. Therefore, the holes (h^+) in the valence band move to the surface and can react with H₂O ($E_{OH/H_2O}^0 = +2.31$ V) form $\cdot OH$ radicals (reaction 4). The agents e^- , h^+ , and $\cdot OH$ are powerful oxidizing and non-selective agents, so they can be degraded and mineralized completely by MB and Ofx to form CO₂, H₂O, and less toxic inorganic products. (reaction 5).



4 Conclusions

In conclusion, CZ catalysts were successfully synthesized by the hydrothermal method with various PVA/Zn²⁺ molar ratios (5, 10, and 15%). The photocatalyst activity of CZ catalysts was accessed through the decomposition of ofloxacin (Ofx) and methylene blue (MB). The results show that the optimal CZ3 catalyst (PVA/Zn²⁺=15%) has about a 2.1 and 2.2 times improvement in the methylene blue and ofloxacin degradation rates compared to that of pure ZnO under visible irradiation. It was found that the C dopant plays an important role in photodegradation because it narrows the band gap energy ($E_{gCZ3} = 2.77 eV$), increases the specific surface area of ZnO ($S_{CZ3} = 26.04 m^2/g$), and the separation of photoelectrons-holes. The results of COD and TOC analysis show that the products of the photodegradation of MB and Ofx are organic molecules with smaller structures. Moreover, the photodegradation reaction mechanism of CZ shows the primary photoactive species were h^+ and $\cdot OH$.

Fig. 11 The photodegradation of **a** MB and **b** Ofx was observed in the presence of radical scavengers and CZ3 under visible light (HL)

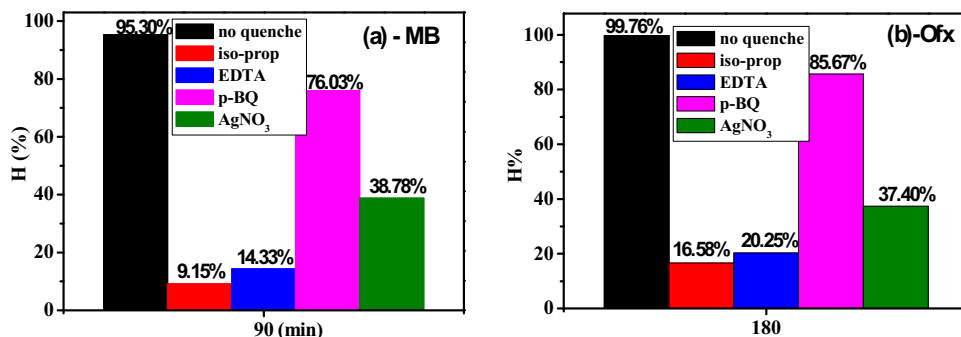
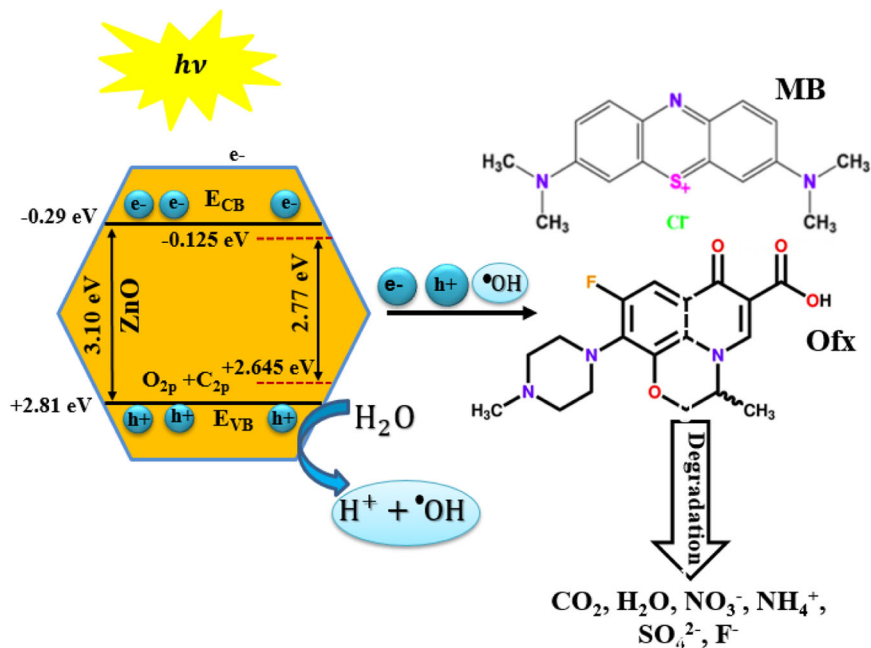


Fig. 12 Schematic illustration of a photocatalytic mechanism for CZ3 nanocatalysts



Author contributions LTVH: Methodology, Writing - original draft, Formal analysis, Validation, Writing - review & editing, Project administration. NTMT: Investigation, Resources. TTTT: Investigation, Resources. LNT: Investigation, Resources. NTD: Data curation, Software. DHP: Writing - review & editing.

Compliance with ethical standards

Conflict of interest The authors declare no competing interests.

Ethics This study does not present research with ethical considerations.

References

- Gaur N, Dutta D, Singh A, et al. (2022) Recent advances in the elimination of persistent organic pollutants by photocatalysis. *Front Environ Sci* 10: <https://doi.org/10.3389/fenvs.2022.872514>
- Alahmadi N (2022) Recent progress in photocatalytic removal of environmental pollution hazards in water using nanostructured materials. *Separations* 9: <https://doi.org/10.3390/separations9100264>
- Nan M, Jin B, Chow CWK, Saint C (2010) Recent developments in photocatalytic water treatment technology: A review. *Water Res.* 44:2997–3027. <https://doi.org/10.1016/j.watres.2010.02.039>
- Kolodziejczak-Radzimska A, Jesionowski T (2014) Zinc oxide—from synthesis to application: A review. *Materials.* 7:2833–2881. <https://doi.org/10.3390/ma7042833>
- Lee JM, Pyun YB, Yi J et al. (2009) ZnO nanorod-graphene hybrid architectures for multifunctional conductors. *J Phys Chem C.* 113:19134–19138. <https://doi.org/10.1021/jp9078713>
- Chen HM, Chen CK, Chang YC et al. (2010) Quantum dot monolayer sensitized ZnO nanowire-array photoelectrodes: True efficiency for water splitting. *Angew Chem - Int Ed* 49:5966–5969. <https://doi.org/10.1002/anie.201001827>
- Lee KM, Lai CW, Ngai KS, Juan JC (2016) Recent developments of zinc oxide based photocatalyst in water treatment technology: A review. *Water Res.* 88:428–448. <https://doi.org/10.1016/j.watres.2015.09.045>
- Mohamed KM, Benitto JJ, Vijaya JJ, Bououdina M (2023) Recent advances in ZnO-based nanostructures for the photocatalytic degradation of hazardous, non-biodegradable medicines. *Crystals* 13: <https://doi.org/10.3390/cryst13020329>
- Kumari H, Sonia, Suman, et al. (2023) A review on photocatalysis used for wastewater treatment: dye degradation. Springer International Publishing.

10. Tanji K, Navio JA, Martín-Gómez AN et al. (2020) Role of Fe(III) in aqueous solution or deposited on ZnO surface in the photoassisted degradation of rhodamine B and caffeine. *Chemosphere* 241:125009. <https://doi.org/10.1016/j.chemosphere.2019.125009>
11. Tanji K, Navio JA, Naja J, et al (2019) Extraordinary visible photocatalytic activity of a Co_{0.2}Zn_{0.8}O system studied in the Remazol BB oxidation. *J Photochem Photobiol A Chem* 382: <https://doi.org/10.1016/j.jphotochem.2019.111877>
12. Belghiti M, Tanji K, El Mersly L et al. (2022) Fast and non-selective photodegradation of basic yellow 28, malachite green, tetracycline, and sulfamethazine using a nanosized ZnO synthesized from zinc ore. *React Kinet, Mech Catal* 135:2265–2278. <https://doi.org/10.1007/s11144-022-02232-8>
13. Yang Y, Li Y, Zhu L et al. (2013) Shape control of colloidal Mn doped ZnO nanocrystals and their visible light photocatalytic properties. *Nanoscale*. 5:10461–10471. <https://doi.org/10.1039/c3nr03160h>
14. Asahi R, Morikawa T, Ohwaki T et al. (2001) Visible-light photocatalysis in nitrogen-doped titanium oxides. *Science* 293:269–271. <https://doi.org/10.1126/science.1061051>
15. Yu W, Zhang J, Peng T (2016) New insight into the enhanced photocatalytic activity of N-, C- and S-doped ZnO photocatalysts. *Appl Catal B* 181:220–227. <https://doi.org/10.1016/j.apcatb.2015.07.031>
16. Liu S, Li C, Yu J, Xiang Q (2011) Improved visible-light photocatalytic activity of porous carbon self-doped ZnO nanosheet-assembled flowers. *CrystEngComm* 13:2533–2541. <https://doi.org/10.1039/c0ce00295j>
17. Haibo O, Feng HJ, Cuiyan L et al. (2013) Synthesis of carbon doped ZnO with a porous structure and its solar-light photocatalytic properties. *Mater Lett* 111:217–220. <https://doi.org/10.1016/j.matlet.2013.08.081>
18. Alshammari AS, Chi L, Chen X et al. (2015) Visible-light photocatalysis on C-doped ZnO derived from polymer-assisted pyrolysis. *RSC Adv* 5:27690–27698. <https://doi.org/10.1039/c4ra17227b>
19. Ansari SA, Ansari SG, Foad H, Cho MH (2017) Facile and sustainable synthesis of carbon-doped ZnO nanostructures towards the superior visible light photocatalytic performance. *N. J Chem* 41:9314–9320. <https://doi.org/10.1039/c6nj04070e>
20. Srinivasan N, Anbuchezhiyan M, Harish S, Ponnusamy S (2019) Applied Surface Science Hydrothermal synthesis of C doped ZnO nanoparticles coupled with BiVO₄ and their photocatalytic performance under the visible light irradiation. *Appl Surf Sci* 494:771–782. <https://doi.org/10.1016/j.apsusc.2019.07.093>
21. Perillo PM, Atia MN (2017) Nano-Structures & Nano-Objects C-doped ZnO nanorods for photocatalytic degradation of p-aminobenzoic acid under sunlight. *Nano-Struct Nano-Objects* 10:125–130. <https://doi.org/10.1016/j.nanoso.2017.04.001>
22. Bechambi O, Sayadi S, Najjar W (2015) Photocatalytic degradation of bisphenol A in the presence of C-doped ZnO: Effect of operational parameters and photodegradation mechanism. *J Ind Eng Chem* 32:201–210. <https://doi.org/10.1016/j.jiec.2015.08.017>
23. Matthews JA (2014) Chemical Oxygen Demand (Cod). *Encyclopedia of Environmental Change* 14–19 <https://doi.org/10.4135/9781446247501.n623>
24. Nezamzadeh-Ejhiieh A, Ghanbari-Mobarakeh Z (2015) Heterogeneous photodegradation of 2,4-dichlorophenol using FeO doped onto nano-particles of zeolite P. *J Ind Eng Chem* 21:668–676. <https://doi.org/10.1016/j.jiec.2014.03.035>
25. Payrazm S, Baghshahi S, Sadeghian Z, Aliabadzadeh A (2022) Structural and optical characterization of ZnO-graphene nanocomposite quantum dots. *Iran J Mater Sci Eng* 19:1–13. <https://doi.org/10.22068/ijmse.2603>
26. Wazir AH, Kundi IW (2016) Synthesis of graphene nano sheets by the rapid reduction of electrochemically exfoliated graphene oxide induced by microwaves. *J Chem Soc Pak* 38:11–16
27. Güell F, Martínez-Alanis PR, Khachadorian S et al. (2016) Raman and photoluminescence properties of ZnO nanowires grown by a catalyst-free vapor-transport process using ZnO nanoparticle seeds. *Phys Status Solidi B Basic Res* 253:883–888. <https://doi.org/10.1002/pssb.201552651>
28. Silambarasan M, Saravanan S, Soga T (2014) Raman and photoluminescence studies of Ag and Fe-doped ZnO nanoparticles. *Int J ChemTech Res* 2014–2015 7(3):1644–1650
29. Beltrán JJ, Barrero CA, Punnoose A (2019) Relationship between ferromagnetism and formation of complex carbon bonds in carbon-doped ZnO powders. *Phys Chem Chem Phys* 21:8808–8819. <https://doi.org/10.1039/c9cp01277j>
30. Sun W, Meng S, Zhang S et al. (2018) Insight into the transfer mechanisms of photogenerated carriers for heterojunction photocatalysts with the analogous positions of valence band and conduction band: a case study of ZnO/TiO₂. *J Phys Chem C* 122:15409–15420. <https://doi.org/10.1021/acs.jpcc.8b03753>
31. Dargahi Z, Asgharzadeh H, Maleki-Ghaleh H (2018) Synthesis of Mo-doped TiO₂/reduced graphene oxide nanocomposite for photoelectrocatalytic applications. *Ceram Int* 44:13015–13023. <https://doi.org/10.1016/j.ceramint.2018.04.120>
32. Maleki-Ghaleh H, Shahzadeh M, Hoseinizadeh SA et al. (2016) Evaluation of the photo-electro-catalytic behavior of nano-structured ZnO films fabricated by electrodeposition process. *Mater Lett*. 169:140–143. <https://doi.org/10.1016/j.matlet.2016.01.090>
33. Mu J, Shao C, Guo Z et al. (2011) High photocatalytic activity of ZnO-carbon nanofiber heteroarchitectures. *ACS Appl Mater Interfaces* 3:590–596. <https://doi.org/10.1021/am101171a>
34. Dillip GR, Banerjee AN, Anitha VC et al. (2016) Oxygen vacancy-induced structural, optical, and enhanced supercapacitive performance of zinc oxide anchored graphitic carbon nanofiber hybrid electrodes. *ACS Appl Mater Interfaces* 8:5025–5039. <https://doi.org/10.1021/acsami.5b12322>
35. Wang J, Wang Z, Huang B et al. (2012) Oxygen vacancy induced band-gap narrowing and enhanced visible light photocatalytic activity of ZnO. *ACS Appl Mater Interfaces* 4:4024–4030. <https://doi.org/10.1021/am300835p>
36. Mishra DK, Mohapatra J, Sharma MK et al. (2013) Carbon doped ZnO: Synthesis, characterization and interpretation. *J Magn Magn Mater* 329:146–152. <https://doi.org/10.1016/j.jmmm.2012.09.058>
37. Tayyebi A, Soltani T, Lee B-K et al. (2017) Novel visible light photocatalytic and Photoelectrochemical (PEC) activity of carbon-doped zinc oxide/reduced graphene oxide: supercritical methanol synthesis with enhanced photocorrosion suppression. *J Alloy Compd* 723:1001–1010. <https://doi.org/10.1016/j.jallcom.2017.06.316>
38. Fu F, Li L, Liu L et al. (2015) Construction of cellulose based ZnO nanocomposite films with antibacterial properties through one-step coagulation. *ACS Appl Mater Interfaces* 7:2597–2606. <https://doi.org/10.1021/am507639b>
39. Okeri HA, Arhewoh IM (2008) Analytical profile of the fluoroquinolone antibacterials. I. Ofloxacin. *Afr J Biotechnol* 7:670–680
40. Jaswal A, Kaur M, Singh S et al. (2021) Adsorptive removal of antibiotic ofloxacin in aqueous phase using rGO-MoS₂ heterostructure. *J Hazard Mater* 417:125982. <https://doi.org/10.1016/j.jhazmat.2021.125982>
41. Sawant SY, Cho MH (2016) Facile and single-step route towards ZnO@C core-shell nanoparticles as an oxygen vacancy induced visible light active photocatalyst using the thermal decomposition of Zn(an)2(NO₃)₂. *RSC Adv* 6:70644–70652. <https://doi.org/10.1039/c6ra14108k>

42. Wang Y, Hu S, Li Q et al. (2018) One step synthesis of high-efficiency AgBr-Br-g-C₃N₄ composite catalysts for photocatalytic H₂O₂ production via two channel pathway. RSC Adv 8:36903–36909. <https://doi.org/10.1039/c8ra07749e>
43. Hinshelwood CN (1945) Physical chemistry. Nature 156:283–284. <https://doi.org/10.1038/156283a0>
44. Dung NT, Thu LM, Thuy UTD et al. (2022) Mechanism insight into the photocatalytic degradation of fluoroquinolone antibiotics by the ZIF-8@Bi₂MoO₆ heterojunction. Environ Sci Nano 9:3973–3991. <https://doi.org/10.1039/d2en00219a>
45. Orange M, Rodwihok C, Wongratanaphisan D, et al. (2020) Cerium-oxide-nanoparticle-decorated zinc oxide with enhanced

photocatalytic degradation of methyl orange. <https://doi.org/10.3390/app10051697>

Publisher's note Springer Nature remains neutral with regard to jurisdictional claims in published maps and institutional affiliations.

Springer Nature or its licensor (e.g. a society or other partner) holds exclusive rights to this article under a publishing agreement with the author(s) or other rightsholder(s); author self-archiving of the accepted manuscript version of this article is solely governed by the terms of such publishing agreement and applicable law.